Phase diagram and thermodynamic model for the Cu-Si and the Cu-Fe-Si systems

Luca Soldi, Annabelle Laplace, Mathieu Roskosz, Stéphane Gossé

Phase diagram and thermodynamic model for the Cu-Si and the Cu-Fe-Si systems

Luca Soldi[1,*], Annabelle Laplace[2], Mathieu Roskosz[3], Stéphane Gossé[1]

[1] DEN-Service de la Corrosion et du Comportement des Matériaux dans leur Environnement (SCCME), CEA, Université Paris Saclay, F-91191, Gif-sur-Yvette, France
[2]DEN- Service d'Etudes de Vitrification et procédés hautes Températures (SEVT), CEA Marcoule, D765, 30200 Chusclan, France
[3] National Museum of Natural History, Institute of Mineralogy, Physics of Materials and Cosmochemistry, Paris, France
[*] Corresponding author: luca.soldi@cea.fr

Abstract
Several processes are designed to treat different type of metallic waste. It is common to find elements like copper, iron and silicon in such systems; the prediction of their behaviour in different conditions can help in improving the efficiency of these treatments. In the present work, the thermodynamic reassessments of the binary Cu-Si and the ternary Cu-Fe-Si systems are proposed. Differential Thermal Analysis and Scanning Electron Microscopy are the techniques adopted to collect new experimental data regarding the transition temperatures and phase equilibria of the investigated systems. The Calphad approach is used to model the phase diagrams of the binary Cu-Si and the ternary Cu-Fe-Si, starting from the new obtained data and the ones available in literature.

Keywords: Calphad; Phase stability; Phase diagram; Thermodynamic properties

1. Introduction

In the framework of metallic waste treatments, the ternary Cu-Fe-Si appears in several applications and processes. Ashes coming from the incineration of domestic waste are in general buried in landfill sites. However, due to the lack of appropriated deposits and the toxicity contained in the residues of such incineration, it might be necessary to melt the bottom ashes and the unburnt waste to reduce their volume, or recover the heavy metals here contained [1–4]. Fe, Cu and glass fragments are mainly found in the remains of the incineration and, during the high temperature treatments, may interact with each other.
In another application, metallic scraps coming from nuclear fuel production are contaminated and classified as Long-Lived Intermediate-Level (LL-IL) nuclear waste. They need treatment in order to confine the radioactive species in a stable matrix before the definitive disposal. A solution consists in melting simultaneously the metallic phase with a silicate glass in order to transfer and confine the active species in the glass matrix. Depending on the waste composition, a large miscibility gap in the liquid phase may lead to the presence of two immiscible metallic liquids: the former heavier and containing mainly Cu; the latter lighter and consisting mostly of Fe.
Besides these applications, the investigated systems plays an important role in the metallurgy and coating of both stainless steels [5–7] and Cu alloys [8,9].
In order to understand all the phenomena that may occur during such processes, it is important to predict well the behaviour and the properties of the ternary Cu-Fe-Si. A thermodynamic description fits perfectly this task and can be implemented to model higher order systems for more complex applications. Here, a new assessment on the Cu-Fe-Si is proposed, starting from an improved model of the binary Cu-Si. Differential Thermal Analysis (DTA) and Scanning Electron Microscopy (SEM) are performed to obtain new experimental data and the results are employed to finalize the thermodynamic descriptions of the binary Cu-Si and the ternary Cu-Fe-Si, thanks to the Calphad (CALculation of PHase Diagram) method [10]. The PARROT module of the software Thermo-Calc is used to optimise the required parameters [11] and then draw the phase diagrams of the investigated systems. The proposed models are then compared with the available data in the literature, finding in general good agreement.

2. Review of literature data

2.1 Cu-Si

The Cu-Si system has been investigated since the beginning of the 20th century because of the technological relevance of its applications, especially in the aluminium and copper metallurgies [12], and it is still crucial nowadays for the development of new types of batteries [13]. Here, a brief overview of the literature is given.

A first comprehensive review of the available data was performed by Olesinski and Abbaschian [14] in 1986, but Rudolfi [15] and Smith [16] already plotted the phase diagram in 1907 and 1928, respectively. Rudolfi investigated the Cu-Si system in the entire domain of compositions, obtaining quite precise results even in the Si-rich side. Smith focused his work on the determination of phase boundaries on the Cu-rich side of the phase diagram. Despite the adopted techniques were characterised by a greater uncertainty than the modern ones, the results of both these works are very reliable and represent important datasets for all the other assessments. More recent works are dedicated to the modelling of this system. Yan and Chang [12] reassessed the thermodynamic description of the Cu-Si binary using the data available in literature. The main differences compared to the previous phase diagram consist in the composition of the hcp phase (richer in Si) and in the description of the phase ε-$Cu_{15}Si_4$.

Shin et al. [17] evaluated the enthalpies of mixing of the solid solutions and the enthalpy of formation ΔH_f of the ε-$Cu_{15}Si_4$ phase through first-principles calculations. In this way, they suggested negative values for the enthalpies of formation also for the other intermetallic compounds, in contrast with the previous models, which adopted positive values. The Special Quasirandom Structures (SQS) [18] approach was used to calculate the enthalpies of mixing for the solid solutions. Computed and experimental data were then taken into account to thermodynamically assess the Cu-rich side of the system (up to 40%$_{at}$ of Si).

The SQS method was also adopted by Wang et al. [19] to predict the enthalpies of mixing in the fcc solid solution. Here, more compositions were investigated compared to the previous calculations of Shin et al. [17], but the results were overall in agreement.

Adachi et al. [20] studied the density and the surface tension of liquid Cu-Si alloys by the electromagnetic levitation method. In order to express the temperature coefficients for both the thermophysical properties investigated, they reported the *liquidus* temperature measured by pyrometry during the experiments. Even if providing thermodynamic data was not the purpose of such work, the *liquidus* temperatures here observed are consistent with the other values found in the literature.

Sufryd et al. [21] conducted an experimental investigation using X-ray diffraction, light optical microscopy, scanning electron microscopy, electron probe microanalysis and differential thermal analysis. More efforts were spent to investigate specific composition ranges regarding the β-bcc, ε-$Cu_{15}Si_4$ and η-Cu_3Si phases and the nature of the invariant equilibria involving the γ-$Cu_{33}Si_7$ ⇄ δ-$Cu_{33}Si_7$ transformation. The results were then employed to draw the phase diagram in the composition range between 70 and 100 %at. Cu, showing an overall agreement with the plot of Olesinski and Abbaschian [14].

Calorimetric measurements were performed by Hallstedt et al. [22] to determine the reaction enthalpies of the invariant reactions involving the liquid phase in the Cu-Si system. Such new data were implemented in a revised thermodynamic model, showing few improvements compared to the work of Shin et al. [17]: better determination of invariant reactions; composition shift for the phase γ-$Cu_{33}Si_7$; allotropic forms of η-Cu_3Si at low temperatures added as different phases; improved partial enthalpies in Si-rich side; inclusion of Cu solubility in diamond-Si phase. However, an anomalous waviness appears in the Si-rich *liquidus*, without a clear explanation.

The present work takes as main reference the model proposed by Hallstedt et al. [22], correcting the inflexion that appears in the Si-rich *liquidus*. The crystallographic information concerning the phases of the Cu-Si binary is reported in Table 1.

Table 1: crystallographic data of the phases in the Cu-Si system.

Phase	Prototype	Space Group	Pearson Symbol	Lattice Parameters / nm			Reference
				a	*b*	*c*	
Fcc	Cu	*Fm-3m*	cF4	0.36149	…	…	[14]
Hcp	Mg	*P6₃/mmc*	hP2	0.25622	…	0.41823	[14]
Bcc	W	*Im-3m*	cI2	0.2854	…	…	[14]
ó-$Cu_{33}Si_7$	-	*P6₃/mmc*	hP*	0.4036	…	0.4943	[23]
γ-$Cu_{33}Si_7$	β-Mn	*P4₁32*	cP20	0.6198	…	…	[14]
ε-$Cu_{15}Si_4$	$Cu_{15}Si_4$	*I-43d*	cI76	0.9718	…	…	[23]
η-Cu_3Si	-	*R-3m*	hR*	0.247	…	…	[24]
η'-Cu_3Si	η'-Cu_3Si	*R-3*	hR9	0.472	…	…	[24]
η''-Cu_3Si	-	?	oC*	7.676	0.700	2.194	[24]
Diamond	C	*Fd-3m*	cF8	0.54306	…	…	[14]

2.2 Cu-Fe-Si

Before proceeding with the literature review of the ternary, two reliable models for the Cu-Fe and the Fe-Si binaries have been chosen for the assessment of the Cu-Fe-Si. Both these binaries are used frequently for modelling higher order systems due to their good quality. Concerning the binary Cu-Fe, the assessment of Ansara [25] (Figure 1A) has been chosen. This system lacks of intermetallic compounds, but is characterised by a metastable liquid miscibility gap, that plays a significant role in the ternary. Regarding the binary Fe-Si, the thermodynamic description proposed by Lacaze and Sundman [26] (Figure 1B) has been selected. They modelled the bcc phase taking into account both the disordered A2 and the ordered B2 contributions. This ordering is included in the present database and correctly calculated only using these binary parameters; for this reason, no distinction between A2 and B2 is made in the ternary optimisation, referring to these phases only as bcc.

Recently, several authors dedicated their researches on the data collection and the thermodynamic description of the ternary Cu-Fe-Si. They especially focused on the influence of the interactions between these elements in the stainless steel metallurgy [6,7,27,28], the properties of copper alloys [9,29], as well as the treatment of the ashes of incinerated waste [1,29].

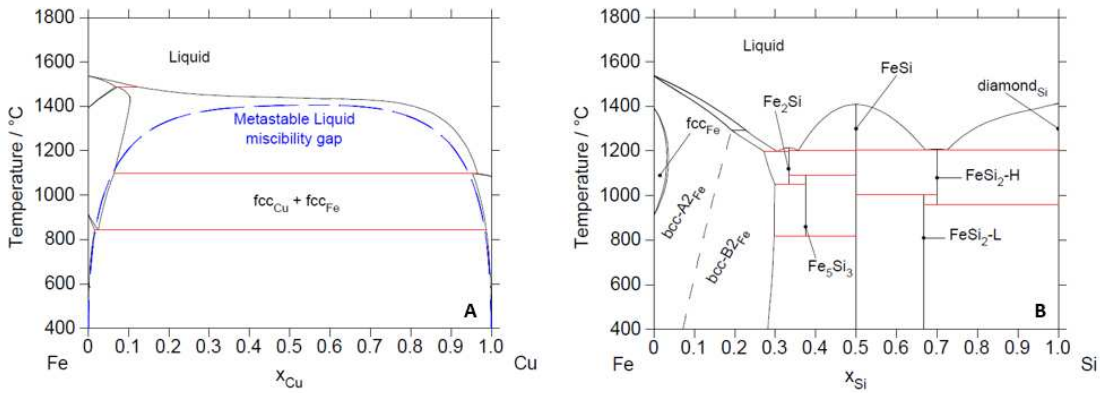

Figure 1 : calculated phase diagrams for the binaries: A) Cu-Fe from Ansara [25], where blue dashed line represents the metastable miscibility gap in the liquid phase; and B) Fe-Si from Lacaze and Sundman [26].

Ohtani et al. [7] studied the solid/liquid equilibria of few ternary systems. Among all, the Cu-Fe-Si was investigated in the Si-poor side at 1100°C, 1200°C and 1300°C and the compositions of liquid and solid phases at the equilibrium were reported. Such data were then used to model the phase diagram at high temperature. No information was reported on intermetallic compounds or specific low temperature equilibria.
A similar study was conducted by Hino et al. [1]. In this research, equilibria at 1250°C, 1350°C and 1450°C are implemented in order to thermodynamically describe the ternary Cu-Fe-Si at high temperature. Here, attention was paid on the large liquid miscibility gap that remains stable up to 1600°C.
Wang et al. [6] studied the compositions of the phases in equilibrium at 800°C, 900°C and 1000°C of four ternaries: Co-Cu-Fe, Cr-Cu-Fe, Cu-Fe-Si and Cu-Fe-V. A thermodynamic model was then proposed for each of these systems in order to fit the available data concerning liquid, bcc and fcc phases.
Miettinen [9] used the available data in literature to optimize the Calphad model of the Cu-Fe-Si. New parameters for liquid and solid solution phases were proposed; the agreement was quite good with all the data implemented.
Another assessment came from Zhao et al. [29]. In this study, samples containing 30 and 70%$_{at}$ Cu were annealed at 750°C for 19 days and analysed by EDX and DTA. These data were then used to assess the phase diagram at high temperatures. Isothermal sections at 1000°C, 1250°C and 1450°C and isopleth at 30 and 70 %$_{at}$ Cu were reported. The model was in overall agreement with the experimental data.
Li and Li [28] analysed the microstructures and the compositions of eleven samples at 650°C by X-Ray Diffraction and Energy Dispersive X-ray spectroscopy; six new three-phase regions were found. These data were used to draw the isothermal section at 650°C, but authors did not assess any thermodynamic model on the Cu-Fe-Si system.

3. Experimental procedure

3.1 Sample preparation

Due to the metallic nature of the investigated systems, the samples were prepared using the arc-melting technique. Ingots of silicon (purity at 99.95%$_{wt}$) copper (99.95%$_{wt}$) and iron (99.9%$_{wt}$) were selected and weighted depending on the established compositions. Then, they were placed in the water-cooled copper crucible of an arc-melting furnace (Edmund Bühler GmbH). After closing the melting chamber, vacuum purges and high-purity argon (99.9999%$_{at}$) refills were performed for three times. Chunks of an oxygen getter (here zirconium) were melted before starting the sample fabrication. These two steps minimise the quantity of the residual oxygen in the chamber and assure a better purity of the samples. In order to maximise the homogeneity of the alloys, they are melted at least three times each. The overall mass loss was always confirmed to be less than 5%. The compositions of all the investigated samples are shown in Table 2 for the Cu-Si binary and in Table 3 for the Cu- Fe-Si ternary.

3.2 Differential Thermal Analysis

The Differential Thermal Analysis (DTA) experiments were performed to measure the transition temperatures thanks to a thermo-balance Setaram Setsys 16/18; alumina crucibles were used. Vacuum purges and high-purity argon refills were repeated three times before starting the analysis in order to minimize the quantity of

Table 2: Sample atomic compositions for Cu-Si binary.

Sample	Composition / %$_{at}$	
	Cu	Si
CuSi-1	68.8	31.2
CuSi-2	68.2	31.8
CuSi-3	68.6	31.4
CuSi-4	72.8	27.2
CuSi-5	63.6	36.4
CuSi-6	65.8	34.2

Table 3: Sample atomic compositions for Cu-Fe-Si ternary.

Sample	Composition / $\%_{at}$		
	Cu	Fe	Si
CuFeSi-1	11.8	41.4	46.8
CuFeSi-2	13.6	22.8	63.6
CuFeSi-3	5.4	87.1	7.5
CuFeSi-4	5.3	88.3	6.4
CuFeSi-5	14.3	16.6	69.1
CuFeSi-6	34.1	38.7	27.2
CuFeSi-7	29.0	31.4	39.6
CuFeSi-8	8.4	53.4	38.2

oxygen that could interact with the sample during the experiment. A constant flow of argon was also granted during the entire analysis. Samples were heated up to 1500°C at rates from 1 to 20 °C/min. The temperature measurements were provided by a thermocouple type B (made by two wires of composition 94%$_{wt}$ Pt, 6%$_{wt}$ Rh and 70%$_{wt}$ Pt, 30%$_{wt}$ Rh), calibrated using aluminium (660.3°C), silver (961.8°C), gold (1064°C) and copper (1085°C) as references; the maximum calibration error was estimated to be 2°C. Such a calibration has been verified regarding the melting point of pure nickel (1455°C), confirming its good quality even at high temperatures.

To determine the temperature at which phase transitions take place, the "first detectable departure from baseline" method was preferred instead the most used linear extrapolation one. In fact, accordingly to Boettinger et al. [30], the latter method is well suited for determining the transition temperatures in pure metals or eutectic alloys, where the onset is quite sharp. However, in case of a general alloy, the baseline close to the transition is not linear, so extrapolating the onset in such condition leads to a larger error (Figure 2).

3.3 Scanning Electron Microscopy and Energy Dispersive X-ray spectroscopy

After the DTA, samples were enrobed in a resin Epofix (Struers) and then polished before being observed at the Scanning Electron Microscope (SEM, Zeiss). Both the secondary electrons (SE) and the backscattered electrons (BSE) modes were adopted. A quantitative evaluation of the phase compositions at room temperature was performed using the Energy Dispersive X-ray spectroscopy (EDX). A tension of 15 keV was employed to both acquire the images and perform the composition measurements; the acquisition time was set to 30 seconds.

4. Experimental results in the Cu-Si system

The compositions of samples concerning the binary Cu-Si are reported in Table 2. The amount of Si was chosen in order to

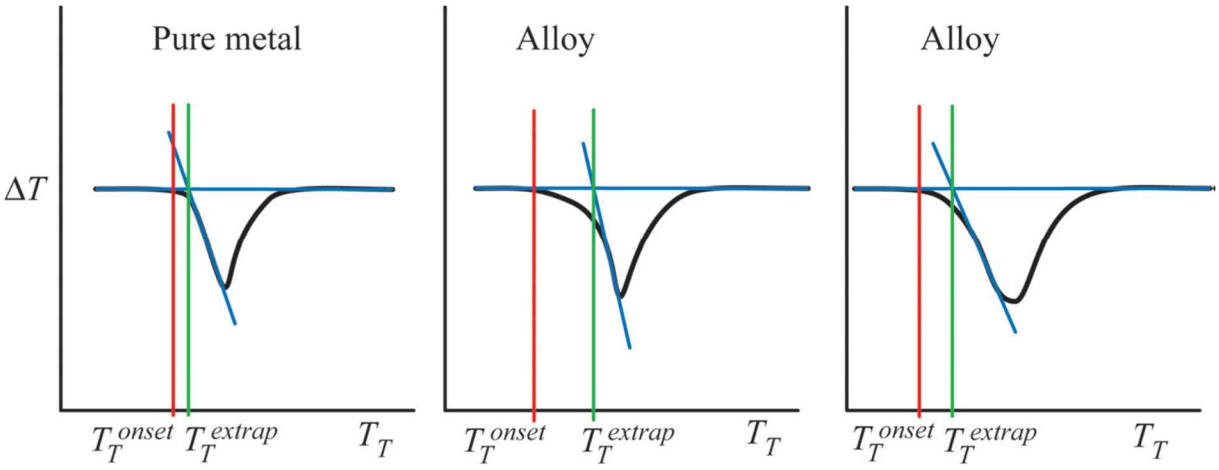

Figure 2 : schematic DTA plots showing error introduced by using the extrapolation method for onset determination (green lines) rather than the first detectable departure from baseline (red lines). They are reported from Boettinger et al. [30].

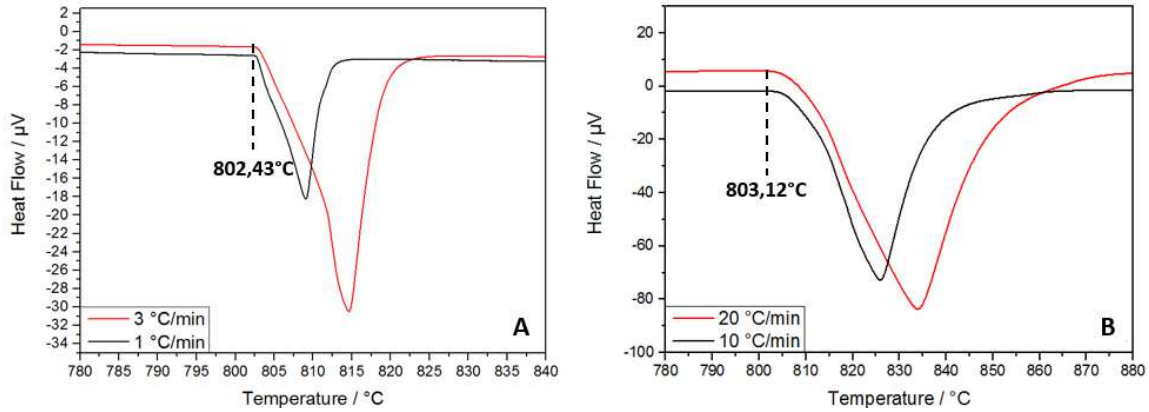

Figure 3 : DTA curves of: A) sample CuSi-1, and B) sample CuSi-3. The curves here reported are obtained with heating rate of 3°C/min (red line) and 1°C/min (black line) for sample CuSi-1, and 20°C/min (red line) and 10°C/min (black line) for sample CuSi-3.

experimentally observe the eutectic reaction expressed in Eq. 1:

$$\text{Liquid} \rightleftarrows \eta\text{-}Cu_3Si + \text{diamond-Si} \qquad (1)$$

In the assessment of Hallstedt et al. [22], the eutectic reaction reported in Eq. 1 is calculated to occur at 31.2%$_{at}$ of Si and at a temperature of 806.4°C.

4.1 Differential Thermal Analysis

In order to determine the temperature of the reaction reported in Eq. 1, two different treatments were foreseen: samples CuSi-1 and CuSi-2 were heated imposing rates of 3 and 1°C/min from 750 to 900°C; the four remaining ones were treated using heating rates of 20 and 10°C/min in the temperature range between 600 and 1000°C.

The curves concerning the samples CuSi-1 and CuSi-3 are reported in Figure 3. Looking at the peaks, two different slopes are recognizable in the left side of each of them, while an invariant reaction (as the one investigated) is characterised by only one. This change in slope may be related to an interaction between the forming liquid and the Al_2O_3 crucible, or to a displacement of the liquid in the crucible. Such behaviour is more evident for lower heating rate. However, even if this interaction takes place, the eutectic reaction of interest does not seem to be affected by this phenomenon. In fact, the transitions are always observed between 802.46°C (Figure 3A) and 803.12°C (Figure 3B). Such values are very consistent one with each other and within the typical DTA experimental error. Moreover, such results are in very good agreement with the values reported in the works of Smith [16], Shin et al. [17], Sufryd et al. [21] and Hallstedt et al. [22].

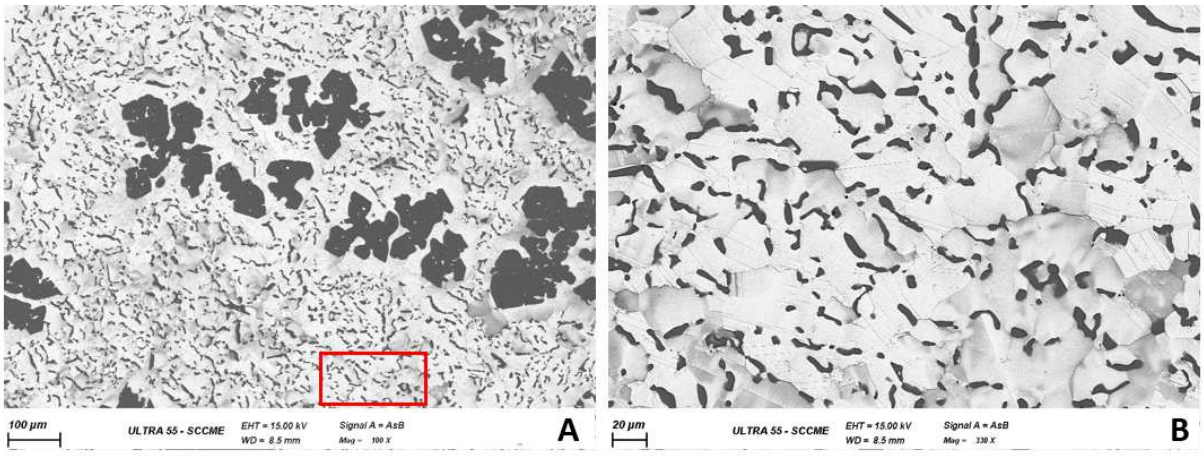

Figure 4 : A) micrograph of sample CuSi-3 and ; B) higher magnification of the red rectangle. The dark dendrites (atomic composition: 1.46% Cu and 98.54%at. Si) embodied in a Cu_3Si-η'' matrix (atomic composition: 78.67% Cu and 21.33% Si) are typical of a eutectic reaction.

4.2 Scanning Electron Microscopy and Energy Dispersive X-ray spectroscopy

All the samples were analysed by SEM in order to determine the phases formed after the treatment. They are all characterised by dark dendrites of Si surrounded by a Cu-rich phases, identified as Cu_3Si (in the η'' allotropic form, stable at room temperature). This structure is compatible with a eutectic transformation, as the one expressed in Eq. 1 and investigated with the DTA. In particular, in sample CuSi-3 the dark dendrites (containing in average 98.54%$_{at}$ Si and 1.46%$_{at}$ Cu) are spread everywhere in the η'' white matrix (formed by 21.33%$_{at}$ Si and 78.67%$_{at}$ Cu), as shown in Figure 4.

5. Experimental results in the Cu-Fe-Si system

5.1 *Differential Thermal Analysis*

Eight samples were produced for the system Cu-Fe-Si; their atomic compositions are reported in Table 3. Such investigated compositions were chosen in order to observe the liquid to solid high temperature transitions.
Sample CuFeSi-1 is characterised by five reactions. Looking at the DTA curves in Figure 5A, one can observe two different kinds of peak. The small ones (at 843, 1030 and 1077°C) are attributed to phase transitions related to changes in the nature of the intermetallic compounds at the equilibrium; the large ones (at 910 and 1343°C) are due to the formation of two different liquids. In particular, the Cu-rich liquid forms at lower temperature, while the Fe-rich one appears at very high temperature. The different shape is related to the latent heat absorbed during the transitions, being in general higher for the formation of liquids than for solid phases.
However, there are transitions in solid phases characterised by a latent heat as the same magnitude as the formation of liquids, as shown in Figure 5B. In fact, the curves of sample CuFeSi-2 at low temperatures are characterised by two pronounced peaks, one being related to the formation of the Cu-rich liquid (at 789°C, as result of the melting of η-Cu_3Si), and the other to the formation of the intermetallic $FeSi_2$-H. These two invariant reactions are well established also in the binaries Cu-Si and Fe-Si. At higher temperature, the wide peak related to the formation of the Fe-rich liquid appears. The minimum of such a peak is the temperature of *liquidus*, measured at 1158°C.
All the transition temperatures measured during the current research are reported in Table 4.

5.2 Scanning Electron Microscopy and Energy Dispersive X-ray spectroscopy

Analysis by EDX is performed on the samples at room temperature, after the treatment in DTA. No ternary intermetallic compounds are detected, in agreement with all the previous experiments and models published in literature. The only observed compounds come from the binaries Cu-Si and Fe-Si.
Figure 6 shows the phases at equilibrium in the samples CuFeSi-2 (A) and CuFeSi-6 (B). Considering CuFeSi-2, the Si-rich diamond (whose atomic composition determined by EDX is 0.26% Cu, 0.40% Fe and 99.34% Si) and the Cu-rich η'' phases (atomic composition: 75.40% Cu, 0.75% Fe and 23.85% Si) are surrounded by a matrix of $FeSi_2$- L (atomic composition: 0.19% Cu, 30.41% Fe and 69.40% Si). Here, the $FeSi_2$-L is the result of the

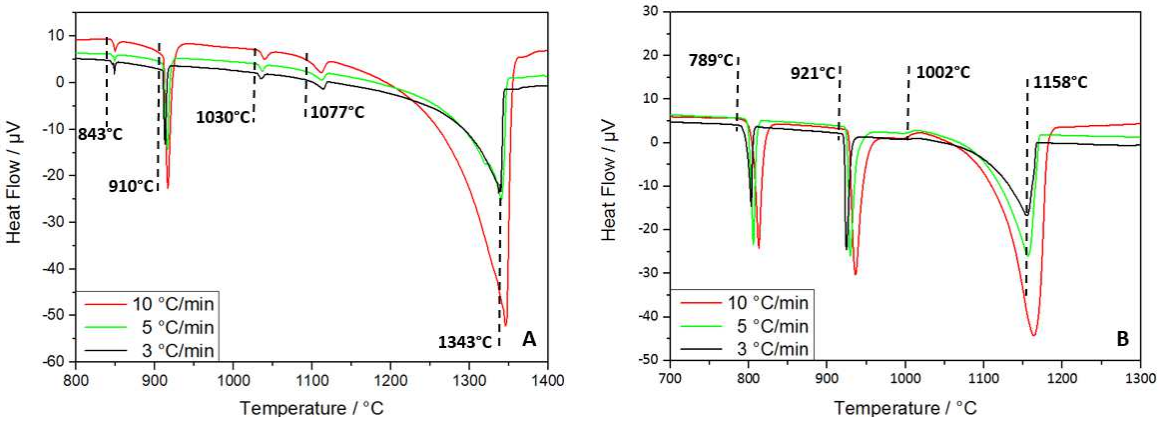

Figure 5 : DTA curves of samples: A) CuFeSi-1; and B) CuFeSi-2. Results obtained at heating rates of 3, 5 and 10 °C/min are shown. Transitions are measured at, respectively, 843, 910, 1030, 1077 and 1343°C, and 789, 921, 1002 and 1158°C. All the transitions are very well reproducible.

Table 4: Transition temperatures about the Cu-Fe-Si ternary obtained by DTA

Sample	Transition temperatures / °C
CuFeSi-1	843 / 910 / 1030 / 1077 / 1343
CuFeSi-2	789 / 921 / 1002 / 1158
CuFeSi-3	1085 / 1428 / 1466
CuFeSi-4	1092 / 1437 / 1474
CuFeSi-5	800 / 920 / 1064 / 1190
CuFeSi-6	906 / 995 / 1032 / 1109 / 1133
CuFeSi-7	815 / 828 / 1290
CuFeSi-8	990 / 1100 / 1135 / 1268

solidification of the Fe-rich liquid that appears in the miscibility gap, while the Cu-rich melt solidifies at lower temperature in the η''. Part of the diamond nucleates directly from the liquid; the remaining is the result of the segregation of Si passing from the phase $FeSi_2$-H (at high temperature) to $FeSi_2$-L (at lower one).
Looking at the phases at room temperature of CuFeSi-6 (Figure 6B), Fe-bcc (characterised by the atomic composition 2.79% Cu, 69.53% Fe and 27.68% Si) is surrounded by a thin layer of FeSi (atomic composition: 2.52% Cu, 47.06% Fe and 50.42% Si) and included in a Cu-fcc matrix (atomic composition: 89.61% Cu, 4.53% Fe and 5.85% Si). In addition, the Fe-rich and the Cu-rich phases come directly from the two immiscible liquids that appear at higher temperature and do not interact each other during the solidification.

6. Thermodynamic modelling

6.1 Calphad method

The Calphad (CALculation of PHAse Diagram) approach is a useful method to perform the thermodynamic modelling of every kind of system. The key point is the calculation of the Gibbs free energy of all the possible phases in a system, fitted from experimental data or calculated thermodynamic properties. All the other thermodynamic functions are then derived from the Gibbs free energy. In particular, minimizing the total Gibbs free energy as function of temperature, pressure and composition of the system allows to determine the thermodynamic equilibria in every condition and to draw phase diagrams [10]. Modelling high-order systems requires an assessment for each sub-system, starting from the pure elements and binaries. In the current work, the module Parrot of the software Thermo-Calc [11] was employed to assess the mathematical parameters

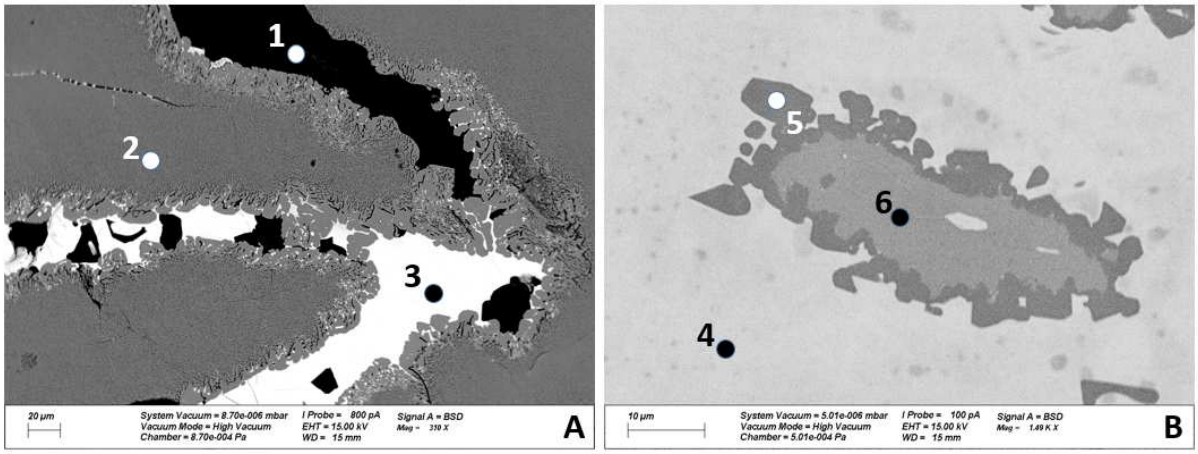

Figure 6 : SEM image of the sample CuFeSi-2 (A) and CuFeSi-6 (B). A: the phases observed in sample CuFeSi-2 are: 1) Si-rich Diamond (atomic compositions by EDX: 0.26% Cu, 0.40% Fe, 99.34% Si); 2) $FeSi_2$-L (atomic composition: 0.19% Cu, 30.41% Fe, 69.40% Si); 3) η''-Cu_3Si (atomic composition: 75.40% Cu, 0.75% Fe, 23.85% Si.
B: Sample CuFeSi-6 is characterised by: 4) Cu-Fcc (atomic composition: 89.61% Cu, 4.53% Fe, 5.85% Si); 5) FeSi (atomic composition: 2.52% Cu, 47.06% Fe, 50.42% Si); 6) Fe-Bcc (atomic composition: 2.79% Cu, 69.53% Fe, 27.68% Si).

using the experimental results described above and the datasets available in literature.
The parameters concerning the Gibbs free energy of the pure elements Cu, Fe and Si come from the SGTE (Scientific Group Thermodata Europe) database realised by Dinsdale [31]. The reference state of molar Gibbs free energy for each element is taken at the standard reference state of the element *i* (i.e. in the stable structure at pressure of 1 bar and temperature of 25°C) and is expressed as $GHSER_i$.
The thermodynamic description of phases appearing in the binaries Cu-Fe are taken by Ansara [25] (Figure 1A). Regarding the Fe-Si binary (Figure 1B), the model proposed by Lacaze and Sundman [26] was preferred to the reassessment of Miettinen [32], because of a better description of the composition of the γ loop in the Fe-rich domain, as well as a better consistency with the experimental data at 800°C provided by Wang et al. [6].

6.2 Cu-Si

The optimised parameters for Cu-Si are listed in Table 5. The solution phases, namely liquid, fcc, bcc and hcp, have been described using the substitutional solution model. Their Gibbs free energy is expressed in Eq. (2):

$$ {}^{0}G^{\varphi}_{\mathrm{Cu,Si}} = x_{\mathrm{Cu}} \cdot {}^{0}G^{\varphi}_{\mathrm{Cu}} + x_{\mathrm{Si}} \cdot {}^{0}G^{\varphi}_{\mathrm{Si}} + R \cdot T \cdot (x_{\mathrm{Cu}} \cdot \ln x_{\mathrm{Cu}} + x_{\mathrm{Si}} \cdot \ln x_{\mathrm{Si}}) + {}^{\mathrm{ex}}G^{\varphi}_{\mathrm{Cu,Si}} \quad (2) $$

where ${}^{0}G^{\varphi}_{\mathrm{Cu,Si}}$ is the molar Gibbs free energy of the solution phase φ taken into account, x_{Cu} and x_{Si} are the molar fractions of Cu and Si respectively, ${}^{0}G^{\varphi}_{\mathrm{Cu}}$ and ${}^{0}G^{\varphi}_{\mathrm{Si}}$ are the molar Gibbs energy of φ containing the pure elements (Cu and Si respectively), R is the gas constant, T the absolute temperature and ${}^{\mathrm{ex}}G^{\varphi}_{\mathrm{Cu,Si}}$ the excess Gibbs energy, describing the interaction between Cu and Si in φ. The expression of ${}^{\mathrm{ex}}G^{\varphi}_{\mathrm{Cu,Si}}$ is given by the Redlich-Kister polynomial [10] in Eq. (3):

$$ {}^{ex}G^{\varphi}_{\mathrm{Cu,Si}} = x_{\mathrm{Cu}} \cdot x_{\mathrm{Si}} \cdot \sum_{n=0}^{\infty} {}^{n}L^{\varphi}_{\mathrm{Cu,Si}} \cdot (x_{\mathrm{Cu}} - x_{\mathrm{Si}})^{n} \quad (3) $$

In the current model, only the liquid phase has parameters up to the second order ${}^{2}L$, the others just need of ${}^{0}L$ and ${}^{1}L$. This choice for the liquid phase leads to an improvement in the description of the *liquidus* in the Si-rich side of the phase diagram.

Table 5: Assessed parameters for the Cu-Si binary.

Phase	Sublattice model	Thermodynamic Parameters in J/mol	Ref.
Liquid	$(Cu,Si)_1$	${}^{0}L^{\mathrm{liq}}_{\mathrm{Cu,Si}}$= -36835+6.92·$T$	This work
		${}^{1}L^{\mathrm{liq}}_{\mathrm{Cu,Si}}$= -46727+19.94·$T$	This work
		${}^{2}L^{\mathrm{liq}}_{\mathrm{Cu,Si}}$= -37886+19.27·$T$	This work
Fcc	$(Cu,Si)_1,Va_1$	${}^{0}L^{\mathrm{fcc}}_{\mathrm{Cu,Si}}$ = -34202+20.5·T	This work
		${}^{1}L^{\mathrm{fcc}}_{\mathrm{Cu,Si}}$ = -47112-5.21·T	This work
Bcc	$(Cu,Si)_1,Va_1$	${}^{0}L^{\mathrm{bcc}}_{\mathrm{Cu,Si}}$ = -15324+15.85·T	This work
		${}^{1}L^{\mathrm{bcc}}_{\mathrm{Cu,Si}}$ = -96059+3.89·T	This work
Hcp	$(Cu,Si)_1,Va_{0.5}$	${}^{0}L^{\mathrm{hcp}}_{\mathrm{Cu,Si}}$ = -27640+19.87·T	This work
		${}^{1}L^{\mathrm{hcp}}_{\mathrm{Cu,Si}}$ = -60580-7.31·T	This work
η-Cu_3Si	$Cu_{0.76}Si_{0.24}$	${}^{0}G^{\eta}_{\mathrm{Cu:Si}}$ = 0.76·$GHSER_{Cu}$+0.24·$GHSER_{Si}$-584.7-6.46·T	This work
η'-Cu_3Si	$Cu_{0.765}Si_{0.235}$	${}^{0}G^{\eta'}_{\mathrm{Cu:Si}}$ = 0.765·$GHSER_{Cu}$+0.235·$GHSER_{Si}$-1402-5.52·T	This work
η''-Cu_3Si	$Cu_{0.77}Si_{0.23}$	${}^{0}G^{\eta''}_{\mathrm{Cu:Si}}$ = 0.77·$GHSER_{Cu}$+0.23·$GHSER_{Si}$-1921-4.88·T	This work
ε-$Cu_{15}Si_4$	$Cu_{15}Si_4$	${}^{0}G^{\varepsilon}_{\mathrm{Cu:Si}}$ = 15·$GHSER_{Cu}$+4·$GHSER_{Si}$-39336-88.32·T	This work
γ-$Cu_{33}Si_7$	$Cu_{33}Si_7$	${}^{0}G^{\gamma}_{\mathrm{Cu:Si}}$ = 33·$GHSER_{Cu}$+7·$GHSER_{Si}$-99152-146.44·T	This work
ó-$Cu_{33}Si_7$	$Cu_{33}Si_7$	${}^{0}G^{\acute{o}}_{\mathrm{Cu:Si}}$= 33·$GHSER_{Cu}$+7·$GHSER_{Si}$-42398-202.86·$T$	This work

Table 6: Assessed parameter for the Cu-Fe-Si ternary.

Phase	Sublattice model	Thermodynamic Parameters in J/mol	Ref.
Liquid	$(Cu,Fe,Si)_1$	${}^0L^{liq}_{Cu,Fe,Si}$ = -4686	This work
Fcc	$(Cu,Fe,Si)_1,Va_1$	${}^0L^{fcc}_{Cu,Fe,Si}$ = -200726+82.52·T	This work
Bcc	$(Cu,Fe,Si)_1,Va_1$	${}^0L^{bcc}_{Cu,Fe,Si}$ = -276822+127.71·T	This work
FeSi	$(Cu,Fe)_1Si_1$	${}^0G^{FeSi}_{Fe:Si}$ = $GHSER_{Fe}$+$GHSER_{Si}$-72761.2+4.44·T	[26]
		${}^0G^{FeSi}_{Cu:Si}$ = $GHSER_{Cu}$+$GHSER_{Si}$+20000	This work
Fe_2Si	$(Cu,Fe)_{0.67}Si_{0.33}$	${}^0G^{Fe_2Si}_{Fe:Si}$ = 0.67·$GHSER_{Fe}$+0.33·$GHSER_{Si}$-23752-3.54·T	[26]
		${}^0G^{Fe_2Si}_{Cu:Si}$ = 0.67·$GHSER_{Cu}$+0.33·$GHSER_{Si}$+10000	This work
Fe_5Si_3	$(Cu,Fe)_5Si_3$	${}^0G^{Fe_5Si_3}_{Fe:Si}$ = 5·$GHSER_{Fe}$+3·$GHSER_{Si}$-241184+2.16·T	[26]
		${}^0G^{Fe_5Si_3}_{Cu:Si}$ = 5·$GHSER_{Cu}$+3·$GHSER_{Si}$+80000	This work

The phases η-Cu_3Si, η'-Cu_3Si, η''-Cu_3Si, ε-$Cu_{15}Si_4$, γ-$Cu_{33}Si_7$ and ó-$Cu_{33}Si_7$ are here considered as stoichiometric compounds. Their Gibbs energy of formation is described as follows in Eq. (4):

$$ {}^0G^{\varphi}_{Cu:Si} = y^{\varphi}_{Cu} \cdot GHSER_{Cu} + y^{\varphi}_{Si} \cdot GHSER_{Si} + \Delta H^{\varphi}_f - T \cdot \Delta S^{\varphi}_f \quad (4) $$

where y^{φ}_{Cu} and y^{φ}_{Si} are the sublattice fractions of Cu and Si, respectively, in the phase φ, ΔH^{φ}_f the enthalpy of formation and ΔS^{φ}_f the entropy of formation.

The mathematical optimisation was performed taking into account the results shown in Section 4 and from the thermal analysis performed by Rudolfi [15], Smith [16], Adachi [20] and Sufryd [21], the calorimetry of Hallstedt [22] and the *ab-initio* calculations of Shin [17] and Wang [19]. All these data are considered consistent each other, without substantial discrepancies. The results concerning the mixing enthalpy in liquid phase coming from Iguchi [33], Castanet [34], Batalin [35] and Witusiewicz [36] are implemented too.

6.3 Cu-Fe-Si

All the parameters optimised for the Cu-Fe-Si are shown in Table 6. Regarding the solution phases (liquid, fcc and bcc), the mathematical equation is expressed in Eq. (5):

$$ \begin{aligned} {}^0G^{\varphi}_{Cu,Fe,Si} = {} & x_{Cu} \cdot {}^0G^{\varphi}_{Cu} + x_{Fe} \cdot {}^0G^{\varphi}_{Fe} + x_{Si} \cdot {}^0G^{\varphi}_{Si} + R \cdot T \cdot (x_{Cu} \cdot \ln x_{Cu} + x_{Fe} \cdot \ln x_{Fe} \\ & + x_{Si} \cdot \ln x_{Si}) + {}^{ex}G^{\varphi}_{Cu,Fe} + {}^{ex}G^{\varphi}_{Cu,Si} + {}^{ex}G^{\varphi}_{Fe,Si} + {}^{ex}G^{\varphi}_{Cu,Fe,Si} \end{aligned} \quad (5) $$

where ${}^{ex}G^{\varphi}_{Cu,Fe}$ and ${}^{ex}G^{\varphi}_{Fe,Si}$ have the same structure as ${}^{ex}G^{\varphi}_{Cu,Si}$ expressed in Eq. (3), and ${}^{ex}G^{\varphi}_{Cu,Fe,Si}$ is the ternary excess Gibbs energy term, the formalism of which can be found well explained by Lukas et al. (chapter 5.6.4 of [10]). For the metallic compounds, the same formalism expressed in Eq. (4) is still valid, because no ternary compounds are found and the solubility of the third element in the binary compounds is not high

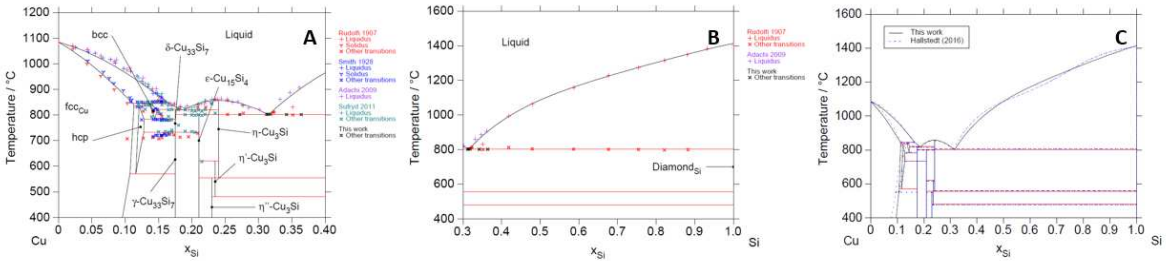

Figure 7 : calculated Cu-Si phase diagram in the present work: A) range of composition between 0 and 40%$_{at}$ Si, compared with experimental data [15,16,20,21]; B) range of composition between 30 and 100%$_{at}$ Si, compared with experimental data [15,20]; C) entire phase diagram in comparison with the model proposed by Hallstedt et al. [22].

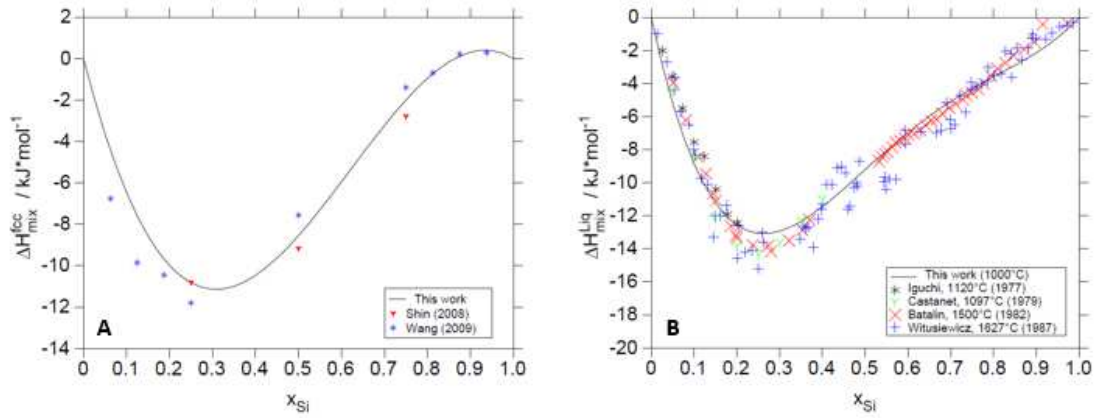

Figure 8 : mixing enthalpy functions for fcc at 25°C (A) and liquid at 1000°C (B) solutions, compared respectively with *ab-initio* data [17, 19] and experimental results [33-36].

enough to introduce interaction parameters.

For the ternary model, the DTA results from Zhao [29], as well as the phase compositions reported by Ohtani [7], Hino [1], Wang [6], Zhao [29] and Li [28] are considered together with the data described in the previous chapter.

7. Discussion

7.1 Cu-Si

The Cu-Si phase diagram resulting from the current modelling is compared with experimental data from Rudolfi [15], Smith [16], Sufryd et al. [21] and Adachi et al. [20] (Figure 7A and Figure 7B) and the model proposed by Hallstedt et al. [22] (Figure 7C). The agreement is overall good with all the datasets and the transitions in the Cu-rich corner of the assessment taken as reference. Moreover, the *liquidus* in the Si-rich side is improved. The mixing enthalpy of the fcc phase is compared with the values computed by Shin et al. [17] and Wang et al. [19] (Figure 8A), while the plot concerning the liquid phase is confronted with the experimental data from Iguchi et al. [33], Castanet [34], Batalin and Sudavtsova [35] and Witusiewicz et al. [36] (Figure 8B). The agreement is overall very good. However, a slight waviness still appears in the mixing enthalpy related to liquid; the *liquidus* modelled by Hallstedt et al. was characterised by a similar behaviour. Theoretically, using a lower number of Redlich-Kister polynomials [10] and lower contributions of the entropic terms to fit the Gibbs free energy should prevent this waviness in the mixing enthalpy of liquid phase. However, the improvement in the current assessment regarding the *liquidus* is consistent, so it should be a better choice for modelling higher order systems based on the binary Cu-Si. All the other reactions are well reproduced, being very close in temperature and composition to the model of Hallstedt et al. [22], taken as reference.

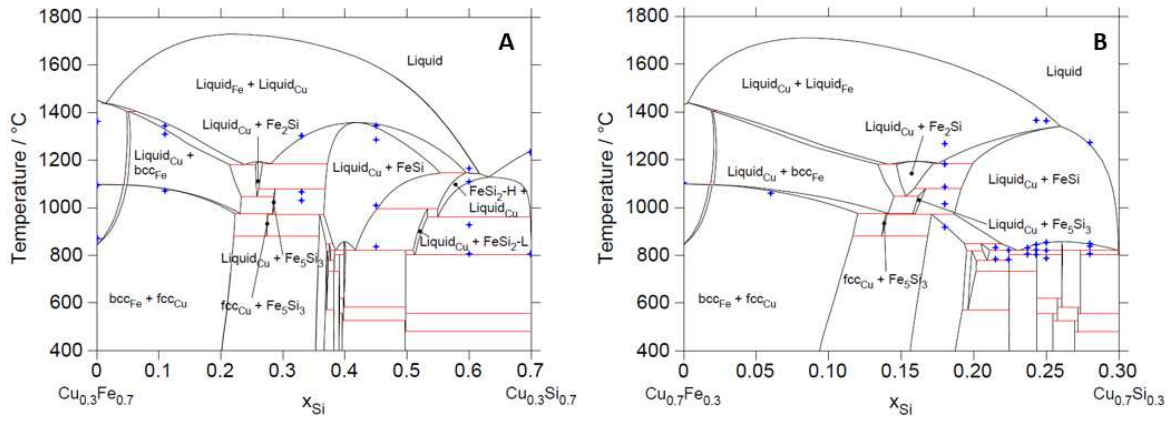

Figure 9 : isopleth sections at: A) 30%$_{at}$ and; B) 70%$_{at}$ Cu of the system Cu-Fe-Si compared with the experimental data of Zhao et al. [29].

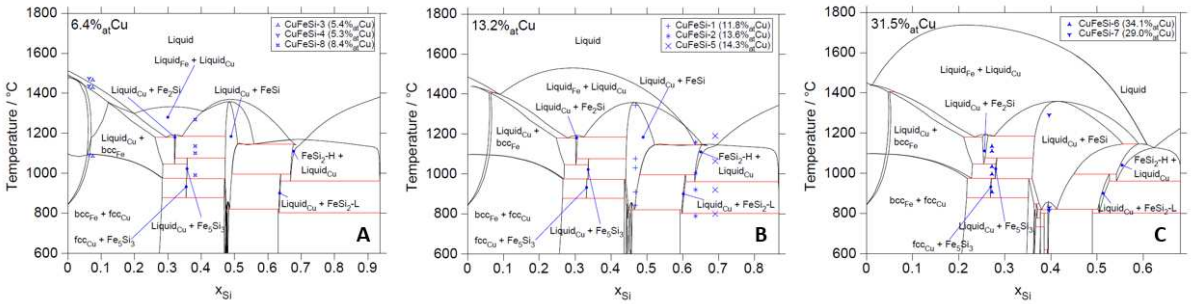

Figure 10 : isopleth sections at : A) 6.4%$_{at}$ Cu ; B)13.2%$_{at}$ Cu ; and C)31.5%$_{at}$ Cu, compared with present experimental data.

7.2 Cu-Fe-Si

The isopleth sections at 30%$_{at}$ and 70%$_{at}$ Cu are compared with the experimental data of Zhao et al. [29] in Figure 9, while isopleth sections at 6.4%$_{at}$, 13.2%$_{at}$ and 31.5%$_{at}$ Cu and the current experimental data are reported in Figure 10. The model predicts very well most of the experimental data available. The major problems regard the transitions involving the intermetallic compounds FeSi and Fe_2Si, mainly due to the binary parameters. In fact, for both these phases, adding a ternary interaction parameter does not affect significantly the transition temperatures coming from the Fe-Si model. Good agreement with the experimental data is found also looking at the isothermal sections at 800, 1250 and 1450°C (Figure 11). Here, the datasets of Wang et al. [6] and Hino et al. [1] are well reproduced by the current assessment. Only the compositions of fcc-Cu solid solution at 800°C differ slightly from the calculations.

The Cu-Fe-Si thermodynamic model here proposed is in overall good agreement with the data available in literature and the experimental results presented. The intermetallic compounds come from the binaries Cu-Si and Fe-Si. A miscibility gap in the liquid phase appears in a wide range of compositions in the Si-poor side, because of the metastable one appearing in the Cu-Fe binary. Looking at the *liquidus* projection of the ternary, two immiscible liquids can be found up to very high temperature (around 1780°C, as shown in Figure 12). Such information is very useful especially to study processes where these metals are melted together. The current description takes into account a better assessment for the Cu-Si binary and, for this reason, shows a better reliability. However, some more improvements may be implemented. For example, more experiments about the composition of the liquids in the miscibility gap would be very useful in order to determine more precisely the limits of the binodal curve.

8. Conclusions

In the current work, the binary Cu-Si and the ternary Cu-Fe-Si have been re-assessed due to the key role played by these systems during the vitrification of LL-IL waste or in the residues of incinerated domestic waste. Experimental data from DTA and SEM-EDX provided new insight for the thermodynamic modelling of these two systems. The binary Cu-Si shows an improvement in the description of the Si-rich *liquidus*, if compared to the model proposed by Hallstedt et al. [22]. This new description has been used to assess the ternary Cu-Fe-Si, characterised by a large miscibility gap in the liquid phase at high temperature. The current model predicts well

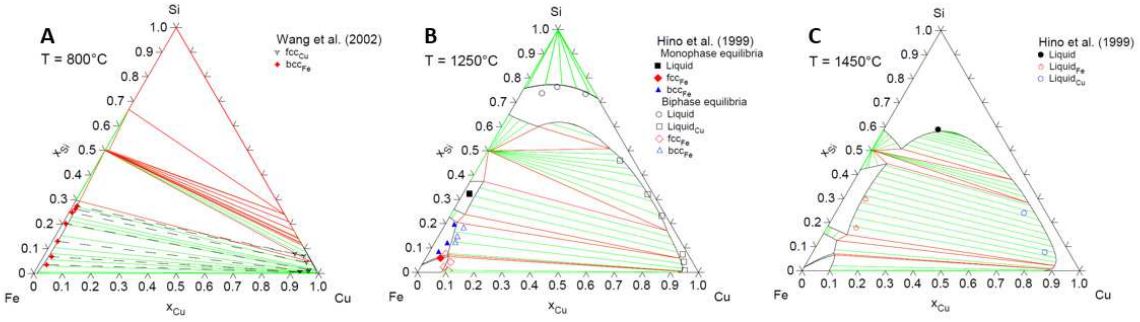

Figure 11 : isothermal sections calculated by the current model at : A) 800°C ; B) 1250°C and C) 1450°C, compared with experimental data from Wang et al. [6] and Hino et al. [1].

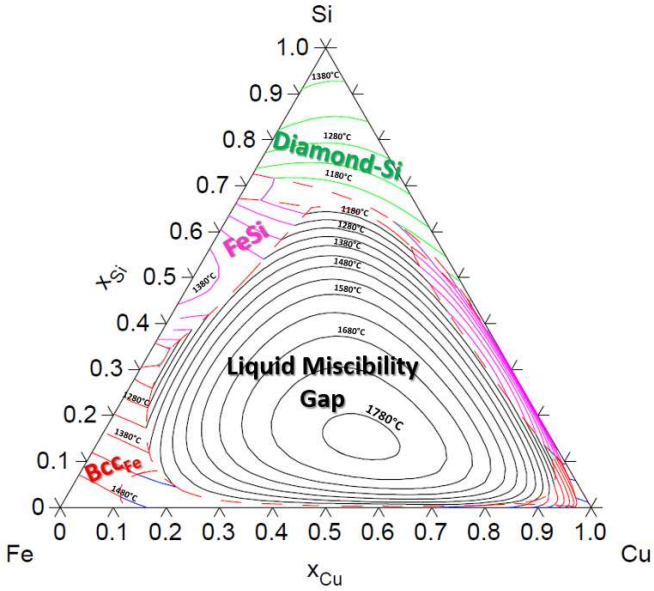

Figure 12 : projection of the liquidus in the Cu-Fe-Si ternary. The large miscibility gap in the liquid phase affects most of the compositions of this system.

the temperature transitions and phase equilibria at the compositions reported in the literature.

References

[1] M. Hino, T. Nagasaka, T. Washizu, Phase diagram of Fe-Cu-Si ternary system above 1523 K, J. Phase Equilibria. 20 (1999) 179. doi:10.1361/105497199770335695.

[2] J. Dong, Y. Chi, Y. Tang, M. Ni, A. Nzihou, E. Weiss-Hortala, Q. Huang, Partitioning of Heavy Metals in Municipal Solid Waste Pyrolysis, Gasification, and Incineration, Energy Fuels. 29 (2015) 7516–7525. doi:10.1021/acs.energyfuels.5b01918.

[3] P.R. Kowalski, M. Kasina, M. Michalik, Metallic Elements Fractionation in Municipal Solid Waste Incineration Residues, Energy Procedia. 97 (2016) 31–36. doi:10.1016/j.egypro.2016.10.013.

[4] S. Patra, S.T. Whaung, W.L. Kwan, Analysis of heavy metals in Incineration Bottom Ash in Singapore and potential impact of pre-sorting on ash quality, Energy Procedia. 143 (2017) 454–459. doi:10.1016/j.egypro.2017.12.710.

[5] P. Li, A. Wang, C.T. Liu, Composition dependence of structure, physical and mechanical properties of FeCoNi(MnAl)x high entropy alloys, Intermetallics. 87 (2017) 21–26. doi:10.1016/j.intermet.2017.04.007.

[6] C.P. Wang, X.J. Liu, I. Ohnuma, R. Kainuma, K. Ishida, Phase equilibria in Fe-Cu-X (X: Co, Cr, Si, V) ternary systems, J. Phase Equilibria. 23 (2002) 236. doi:10.1361/105497102770331712.

[7] H. Ohtani, H. Suda, K. Ishida, Solid/Liquid equilibria in Fe-Cu based ternary systems, ISIJ Int. 37 (1997) 207–216.

[8] T. Hidayat, D. Shishin, S.A. Decterov, E. Jak, Critical assessment and thermodynamic modeling of the Cu–Fe–O–Si system, Calphad. 58 (2017) 101–114. doi:10.1016/j.calphad.2017.06.003.

[9] J. Miettinen, Thermodynamic description of the Cu–Fe–Si system at the Cu–Fe side, Calphad. 27 (2003) 389–394. doi:10.1016/j.calphad.2004.01.003.

[10] H.L. Lukas, S.G. Fries, B. Sundman, Computational thermodynamics: the CALPHAD method, Cambridge University Press, Cambridge ; New York, 2007.

[11] B. Sundman, B. Jansson, J.-O. Andersson, The Thermo-calc databank system, Calphad. 9 (1985) 153–190.

[12] X. Yan, Y.A. Chang, A thermodynamic analysis of the Cu–Si system, J. Alloys Compd. 308 (2000) 221–229. doi:10.1016/S0925-8388(00)00983-X.

[13] W. Gierlotka, Md. Azizul Haque, On the binary (Cu+Si) system: Thermodynamic modelling of the phase diagram and atomic mobility in face centred cubic phase, J. Chem. Thermodyn. 57 (2013) 32–38. doi:10.1016/j.jct.2012.07.025.

[14] R.W. Olesinski, G.J. Abbaschian, The Cu-Si (Copper-Silicon) System, Bullettin Alloy Phase Diagr. 7 (1986) 170–178.
[15] E. Rudolfi, Metallographische Mitteilungen aus dem Institut für anorganische Chemie der Universität Göttingen. XLIII. Die Silicide des Kupfers, Z. Für Anorg. Chem. 53 (1907) 216–227. doi:10.1002/zaac.19070530115.
[16] C.S. Smith, The alpha-based boundary of the copper-silicon system, J. Inst. Met. 40 (1928) 359–373.
[17] D. Shin, J.E. Saal, Z.-K. Liu, Thermodynamic modeling of the Cu–Si system, Calphad. 32 (2008) 520–526. doi:10.1016/j.calphad.2008.05.003.
[18] A. Zunger, S.-H. Wei, L.G. Ferreira, J.E. Bernard, Special quasirandom structures, Phys. Rev. Lett. 65 (1990) 353–356. doi:10.1103/PhysRevLett.65.353.
[19] A. Wang, L. Zhou, Y. Kong, Y. Du, Z.-K. Liu, S.-L. Shang, Y. Ouyang, J. Wang, L. Zhang, J. Wang, First-principles study of binary special quasirandom structures for the Al–Cu, Al–Si, Cu–Si, and Mg–Si systems, Calphad. 33 (2009) 769–773. doi:10.1016/j.calphad.2009.10.007.
[20] M. Adachi, M. Schick, J. Brillo, I. Egry, M. Watanabe, Surface tension and density measurement of liquid Si–Cu binary alloys, J. Mater. Sci. 45 (2010) 2002–2008. doi:10.1007/s10853-009-4149-5.
[21] K. Sufryd, N. Ponweiser, P. Riani, K.W. Richter, G. Cacciamani, Experimental investigation of the Cu–Si phase diagram at x(Cu)>0.72, Intermetallics. 19 (2011) 1479–1488. doi:10.1016/j.intermet.2011.05.017.
[22] B. Hallstedt, J. Gröbner, M. Hampl, R. Schmid-Fetzer, Calorimetric measurements and assessment of the binary Cu–Si and ternary Al–Cu–Si phase diagrams, Calphad. 53 (2016) 25–38. doi:10.1016/j.calphad.2016.03.002.
[23] N. Mattern, R. Seyrich, L. Wilde, C. Baehtz, M. Knapp, J. Acker, Phase formation of rapidly quenched Cu–Si alloys, J. Alloys Compd. 429 (2007) 211–215. doi:10.1016/j.jallcom.2006.04.046.
[24] J.K. Solberg, The crystal structure of n-Cu3Si Precipitates in Silicon, Acta Crystallogr. A34 (1978) 684–698.
[25] I. Ansara, Europäische Gemeinschaften, eds., Definition of thermochemical and thermophysical properties to provide a database for the development of new light alloys:: COST 507. Vol. 2: Thermochemical database for light metal alloys, Off. for Off. Publ. of the Europ. Communities, Luxembourg, 1998.
[26] J. Lacaze, B. Sundman, An assessment of the Fe-C-Si system, Metall. Trans. A. 22 (1991) 2211–2223. doi:10.1007/BF02664987.
[27] C.P. Wang, X.J. Liu, I. Ohnuma, R. Kainuma, K. Ishida, Thermodynamic Database of the Phase Diagrams in Cu-Fe Base Ternary Systems, J. Phase Equilibria Diffus. 25 (2004) 320–328. doi:10.1361/15477030420098.
[28] X. Li, Z. Li, Experimental Investigation of the 650 °C Isothermal Section of the Cu-Fe-Si Ternary Phase Diagram, J. Phase Equilibria Diffus. 38 (2017) 94–101. doi:10.1007/s11669-017-0519-x.
[29] J. Zhao, L. Zhang, Y. Du, H. Xu, J. Liang, B. Huang, Experimental Investigation and Thermodynamic Reassessment of the Cu-Fe-Si System, Metall. Mater. Trans. A. 40 (2009) 1811–1825. doi:10.1007/s11661-009-9877-2.
[30] W.J. Boettinger, U.R. Kattner, J.H. Perepezko, DTA and Heat-flux DSC Measurements of Alloy Melting and Freezing, National Institute of Standars and Technology, Special Publication 960-15, Washington 2006.
[31] A.T. Dinsdale, SGTE data for pure elements, version 4.5, Private Communication, Unpublished, (2006).
[32] J. Miettinen, Reassessed thermodynamic solution phase data for ternary Fe-Si-C system, Calphad. 22 (1998) 231–256. doi:10.1016/S0364-5916(98)00026-1.
[33] Y. Iguchi, H. Shimoji, S. Ban-Ya, T. Fuwa, Calorimetric study of heat of mixing of copper alloy at 1120°C, Tetsu--Hagane. 63 (1977) 275–284.
[34] R. Castanet, Thermodynamic investigation of copper + silicon melts, J. Chem. Thermodyn. 11 (1979) 787–791.
[35] G. Batalin, V.S. Sudavtsova, Thermodynamic properties of liquid alloys of the copper silicon system, Inorg. Mater. 18 (1982) 133–135.
[36] V.T. Witusiewicz, I. Apshofen, F. Sommer, Thermodynamics of liquid Cu-Si and Cu-Zr alloys, Z. Fuer Met. 88 (1997) 866–872.